Forced Oscillation Dynamics of Surface Nanobubbles

Forced Oscillation Dynamics of Surface Nanobubbles

Duncan Dockar,[a] Livio Gibelli, and Matthew K. Borg
School of Engineering, Institute of Multiscale Thermofluids, The University of Edinburgh, Edinburgh EH9 3FB, UK

(Dated: 8 October 2020)

Surface nanobubbles have potential applications in manipulation of nanoscale and biological materials, waste-water treatment and surface cleaning. These spherically capped bubbles of gas can exist in stable diffusive equilibrium on chemically patterned or rough hydrophobic surfaces, under supersaturated conditions. Previous studies have investigated their long-term response to pressure variations, which is governed by the surrounding liquid's local supersaturation, however, not much is known about their short-term response to rapid pressure changes, i.e. their cavitation dynamics. Here, we present Molecular Dynamics simulations of a surface nanobubble subjected to an external oscillating pressure field. The surface nanobubble is found to oscillate with a pinned contact line, while still retaining a mostly spherical cap shape. The amplitude frequency response is typical of an underdamped system, with a peak amplitude near the estimated natural frequency, despite the strong viscous effects at the nanoscale. This peak is enhanced by the surface nanobubble's high internal gas pressure, a result of the Laplace pressure. We find that accurately capturing the gas pressure, bubble volume and pinned growth mode is important for estimating the natural frequency, and we propose a simple model for the surface nanobubble frequency response, with comparisons made to other common models for a spherical bubble, a constant contact angle surface bubble, and a bubble entrapped within a cylindrical micropore. This work reveals the initial stages of growth of cavitation nanobubbles on surfaces, common in heterogeneous nucleation, where classical models based on spherical bubble growth break down.

I. INTRODUCTION

Rapid variations in pressure can spontaneously form bubbles of vapor or gas within a liquid, in a phenomenon known as cavitation. The repeated formation and subsequent collapse of these bubbles usually causes problems in engineering, such as in premature wear of turbomachinery.[1] However, at the micro- and nano-scale, these collapsing bubbles have value in applying powerful, controlled liquid jets onto specific targets, which can be used for cancer treatment,[2,3] enhanced gene and drug delivery,[4] waste-water cleaning[5,6], nanomaterial fabrication,[7–9] and complex geometry surface cleaning.[10] Other interesting applications depend on the oscillatory dynamics of these cavitating bubbles, such as in ultrasound contrast agents, where the natural frequency of the bubble strengthens the signal in medical imaging.[11,12]

The most commonly used model for the dynamics of a *spherical* bubble in the bulk, as shown in Fig. 1(a), is the Rayleigh–Plesset equation:

$$R\ddot{R}+\frac{3}{2}\dot{R}^2+\frac{4\nu\dot{R}}{R}=\frac{1}{\rho}\left[P_{g,0}\left(\frac{R_0}{R}\right)^{3k}-(P_\infty-P_v)-\frac{2\gamma}{R}\right], \tag{1}$$

where ρ and ν are the liquid density and kinematic viscosity, respectively; R is the radius of the bubble, with initial radius, R_0; $P_{g,0}$, P_∞, and P_v are the initial gas pressure, far-field liquid pressure, and vapor pressure, respectively; γ is the liquid–gas surface tension; k is the exponent of the polytropic gas law, $P_gV^k=$ const., where V is the bubble volume.[1,13] Dot notation is used to indicate time-derivatives, e.g. $\mathrm{d}R/\mathrm{d}t=\dot{R}$, and $\mathrm{d}^2R/\mathrm{d}t^2=\ddot{R}$.

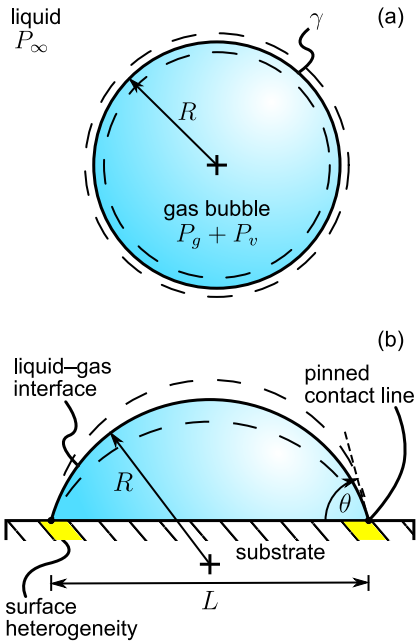

FIG. 1: Schematics of: (a) a spherical bubble, and (b) a surface nanobubble, under forced oscillation.

One of the strengths of Eq. (1) is its ability to capture the rapid bubble dynamics over large changes in scale common in cavitation, for example, in the unstable growth and collapse phases, which can be difficult to fully observe in other simulation and experimental methods.[14–17] The Rayleigh–Plesset equation has also been shown to give good agreement with hydrodynamic based simulations of vapor bubble formation around heated nanoparticles,[18] and free oscillations of microbubbles with Reynolds numbers as low as $Re=10$.[19] Re-

[a]Electronic mail: d.dockar@ed.ac.uk

cently, several authors have started using Rayleigh–Plesset dynamics to model viscous dominated spherical nanobubbles with Molecular Dynamics (MD) simulations.[20–23]

Surface nanobubbles are spherical cap shaped bubbles pinned to a surface with sizes in the nanometre range, as shown in Fig. 1(b). They have been shown to exist stably on textured or rough hydrophobic surfaces in supersaturated solutions, for up to hours or days at a time.[9,24–31] Since only being discovered relatively recently, their cavitation dynamics are still not fully understood. For example, the threshold liquid pressure at which they experience unstable growth was found to be lower than the classical Blake threshold for spherical bubbles.[32,33] This discrepancy has been previously shown to be due to the pinning of the three-phase contact line causing a reduction in surface nanobubble radius of curvature during constant contact radius (CCR) growth, as well as a different expression for their spherical cap volume. This CCR growth mode also means that Eq. (1), which assumes radial growth, is unsuitable for modeling the growth rate and oscillation dynamics of surface nanobubbles. The natural frequencies of spherical bubbles,[34–36] constant contact angle (CCA) surface bubbles,[37] constrained spherical bubbles,[38] and gas bubbles entrapped within micropores[39,40] have been previously investigated, however, there have been no studies specifically on the oscillating dynamics of surface nanobubbles.

Future technologies that rely on the cavitation dynamics of these surface nanobubbles, such as in ultrasound contrast agents or surface cleaning, require understanding of their oscillation and growth rates. In this work, we model the forced oscillation dynamics of a surface nanobubble at varying frequencies, investigate the oscillation shape and pressure balances across the interface, and compare different models to predict the bubble's natural frequency.

It is necessary to fully capture the complex physics behind surface nanobubbles, in order to clarify the many unclear aspects of their dynamics. MD is a high-fidelity simulation technique that can model such behavior, for example, the contact line stick/slip dynamics, surface tension effects and diffusive growth, via fundamental Newtonian dynamics and chemical intermolecular potentials.[33,41–44] The penalty of MD is its extreme computational cost, which limits the bubble sizes that can be modeled ($R \sim 10\,\text{nm}$) as well as the largest time scales of the dynamics ($\sim 10\,\text{ns}$). Other techniques exist for modeling surface nanobubbles, such as lattice density functional theory,[26] and more recently with continuum-based solvers, coupling a finite difference scheme with the immersed boundary method to simulate pinned growth under various saturation conditions for μm sized surface nanobubbles.[45] However, these alternative techniques usually take assumptions on the bubble's growth, for example that the contact line is pinned, which is not yet known to be true for the rapid oscillations to be modeled here, and so we chose MD to accurately capture this growth mode.

II. MOLECULAR DYNAMICS SIMULATION SETUP

We performed simulations of pinned surface nanobubble growth using the LAMMPS MD software[46] with pressures enforced at varying frequencies. The fluid system employed was nitrogen (N_2) for the internal gas phase, and water (H_2O) for the external liquid, given that this combination is common in surface nanobubble literature.[9,24,47,48] The fluid domain was contained between two walls, with the liquid pressure controlled by vertical motion of the upper wall (referred from now on as the piston), and the bubble equilibrated on the lower rigid wall, as shown in Fig. 2, with an enhanced view of the bubble shown in inset A. Contact line pinning was provided by a concentric ring pattern of alternating hydrophobic (S_o) and hydrophilic (S_i) atom types (similar to our previous simulation setup in Ref. 33), directly below the surface nanobubble, as shown in inset B.[49]

We performed simulations using the coarse-grained mW model for the liquid,[51] and a neutral single-site N_2 model for the gas,[52] with relative potential parameters chosen based on gas solubility.[53] The mW model was chosen for its good agreement with water density and surface tension at ambient conditions. It is also computationally cheaper than other standard MD water models such as TIP4P/2005,[54] although does underpredict viscosity.[55] The computational gains allowed us to study large liquid baths surrounding the nanobubble, which was important for capturing the full inertial and viscous contributions from the surrounding liquid. Interatomic interactions between the mW molecules were modeled using the Stillinger–Weber (SW) potential:[56]

$$U_{SW} = \sum_i \sum_{j>i} A_s \varepsilon_{ij} \left[B_s \left(\frac{\sigma_{ij}}{r_{ij}} \right)^{p_s} - \left(\frac{\sigma_{ij}}{r_{ij}} \right)^{q_s} \right] \exp\left(\frac{\sigma_{ij}}{r_{ij} - a_s \sigma_{ij}} \right) + \sum_i \sum_{j \neq i} \sum_{k>j} \lambda_s \varepsilon_{ijk} \left[\cos\theta_{jik} - \cos\theta_s \right]^2 \exp\left(\frac{\gamma_s \sigma_{ij}}{r_{ij} - a_s \sigma_{ij}} \right) \exp\left(\frac{\gamma_s \sigma_{ik}}{r_{ik} - a_s \sigma_{ik}} \right), \tag{2}$$

where U_{SW} is the total potential energy between the system of atoms interacting by the SW potential;[57] atoms i and j are separated by distance r_{ij}, and likewise atoms i and k are separated by distance r_{ik}; atoms j and k form an angle θ_{jik}, subtended at atom i; ε and σ are the characteristic potential depth and length-scale, respectively, with the subscripts denoting the atomic combinations. The fitting parameters A_s, B_s, a_s, p_s, q_s, λ_s, θ_s and γ_s are chosen to achieve fluid properties similar to water, and are given in Table I. Potential parameters ε and σ are given in Table II.

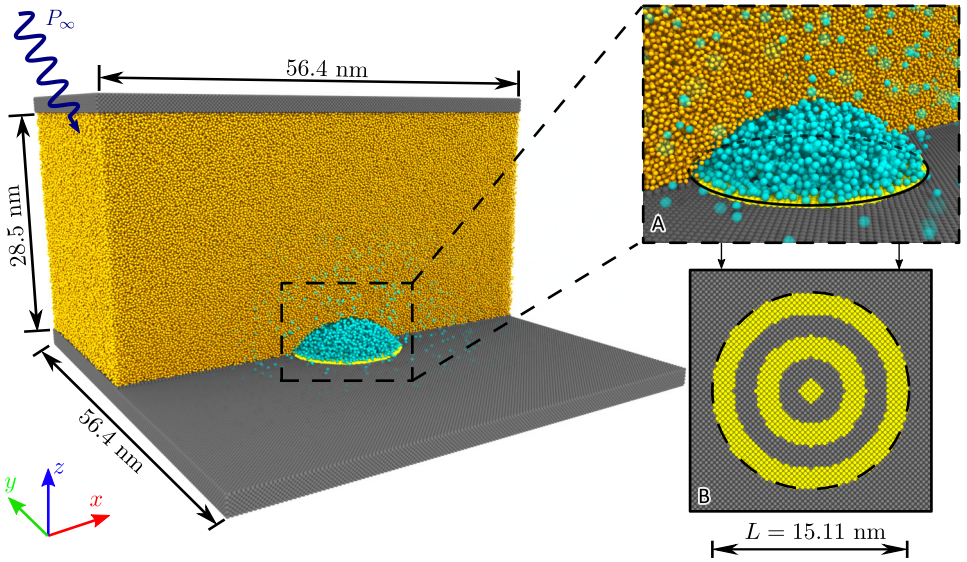

FIG. 2: Schematic of the MD simulation of a 3D surface nanobubble. The orange spheres are the single-site mW water molecules, cyan spheres are the single-site N_2 molecules, and the dark-grey and yellow atoms are the hydrophilic (S_i) and hydrophobic (S_o) substrate sections, respectively.[50] Some of the mW molecules and dissolved N_2 molecules are not shown for clarity. Inset A shows the surface nanobubble in more detail, and inset B shows the S_i/S_o substrate patterning directly below the bubble.

TABLE I: Fitting parameters used in Eq. (2) to obtain a coarse-grained model for monatomic water.[51]

Fitting parameter	Value
A_s	7.049 556 27
B_s	0.602 224 558 4
a_s	1.8
p_s	4
q_s	0
λ_s	23.15
θ_s	109.47°
γ_s	1.2

TABLE II: Atom types and parameters for interatomic potential interactions; parameters for atoms in bold are assumed for pairs of like atoms. Any interaction pairs not given are equal to zero.

Atom/ Interatomic pair	Atom Mass (g/mol)	ε (kJ/mol)	σ (nm)
mW[a]	18.015	25.895	0.23925
mW–N_2	–	0.41250	0.30713
mW–S_o	–	0.90332	0.24318
mW–S_i	–	1.8995	0.24318
N_2[b]	28.013	0.79160	0.37500
N_2–S_o	–	2.3334	0.31105
N_2–S_i	–	1.1051	0.31105

[a] Ref. 51
[b] Ref. 52

All other interatomic interactions, including interactions between the water molecules and other atoms/molecules in the system, were modeled using the Lennard Jones (LJ) potential:

$$U_{LJ} = \sum_i \sum_{j>i} 4\varepsilon_{ij} \left[\left(\frac{\sigma_{ij}}{r_{ij}} \right)^{12} - \left(\frac{\sigma_{ij}}{r_{ij}} \right)^{6} \right], \qquad (3)$$

where U_{LJ} is the total potential energy from all the LJ potential interactions; ε_{ij} and σ_{ij} are the characteristic potential and length-scale, respectively, between atoms i and j. The LJ potential pair parameters used for the mW and N_2 model simulations are also shown in Table II, using similar values from past surface nanobubble simulations.[33,42,43] Potential parameters between mW molecules and the S_o and S_i atom types were calibrated in pre-simulations to obtain equilibrium gas-side contact angles of 35° and 99°, respectively. Potential parameters between the nitrogen molecules and the wall atom types were calibrated to achieve similar density fluctuation profiles as found in Refs. 33, 42, and 43.

Pressure was applied by the piston, with all piston atoms subjected to a mean force $F_z = -P_\infty A_p/N$, where A_p is the area of the piston in the (x, y) plane, and N is the number of piston wall atoms. The negative sign indicates that for a positive pressure, the force on the piston acts downwards, i.e. in the negative z direction. Periodic boundaries were applied in the x and y directions, while non-periodic boundaries were used in the z direction.

All simulations started from an identical equilibrated state, which was first achieved by initializing the bubble as a spherical cap shape (to reduce diffusive equilibration time), with 3×10^6 water molecules for the bulk liquid, 7700 gas molecules in the bubble, and a further

1872 nitrogen molecules dissolved in the liquid to provide supersaturation.[28,33,42,58,59] Equilibration was performed at constant temperature $T = 300\,\mathrm{K}$ using a Nosé–Hoover thermostat[46,60,61] and at constant initial pressure $P_{\infty,0} = 10\,\mathrm{MPa}$ (using the piston), until the bubble had reached a steady size after 1.5 ns, with initial gas-side contact angle[62] $\theta_0 = 50.5^\circ$ and lateral contact diameter $L = 15.11\,\mathrm{nm}$. The equilibrated fluid domain measured $56.4 \times 56.4 \times 28.5\,\mathrm{nm}^3$, although could expand in the z direction to allow variations in pressure. The piston comprised of 3.73×10^5 S_i atoms, with a total mass: $m_p = 1.21 \times 10^{-19}\,\mathrm{kg}$.

Pressure could be measured in the gas and liquid phases using the combined kinetic and virial stress tensor,[46,63] and was confirmed to reach equilibrium values after this time. During the main production MD runs, the thermostat was applied only to the liquid, which allowed the nitrogen gas phase to expand without enforcing an adiabatic or isothermal behavior.[33] The velocity Verlet algorithm was used,[46] with a time-integration step of $\Delta t = 2\,\mathrm{fs}$ for all simulations.

Relevant parameters of the mW liquid were obtained from MD pre-simulations, all at 300 K: surface tension was measured from a simple plane interface system under equilibrium conditions, $\gamma = 65.384\,\mathrm{mJ/m^2}$;[44,64] the dynamic viscosity of the liquid was measured using the Green–Kubo method[65–67], $\mu = 3.550 \times 10^{-4}\,\mathrm{Pa\,s}$; density was assumed constant, $\rho = 1000\,\mathrm{kg/m^3}$;[55] vapor pressure of the liquid at 300 K was assumed $P_v = 3.353\,68 \times 10^{-3}\,\mathrm{MPa}$.[55]

The volume of the bubble as it changed with time could be measured as the volume underneath the normalized 50 % isodensity surface contour. A spherical cap profile was fitted to this surface contour to measure the contact angle, radius of curvature and lateral contact diameter during growth.

Accurate analysis of the surface nanobubble's oscillations requires a semi-infinite domain,[39,40,68] which is difficult to achieve in MD simulations. With computational constraints, a finite number of molecules were used, which could lead to possible discrepancies. In order to minimize these effects, a new length scale was derived in the supplementary material, to evaluate the far-field limit r_∞ at which the inertial effects of the liquid are uninhibited by the domain's limited size. We estimate a minimum size $r_\infty \gg [\Delta P_\infty \rho R_0^6 / 32\mu^2]^{1/4} \approx 2\,\mathrm{nm}$, for our simulations. Despite being an analysis on the inertial effects of the surrounding liquid, the viscosity has a significant role, as it dictates the amplitudes of the bubble oscillations during pressure-driven dynamics. This limit was derived strictly for a spherical bubble, however it can give a rough estimate for a surface nanobubble simulation by setting $R_0 = R_{eq,0}$, where $R_{eq,0} = (3V_0/4\pi)^{1/3}$ (see Section III). In practical terms, r_∞ can be thought of the distance to the closest domain boundary. We suggest the 28.5 nm lengths of our domain, as shown in Fig. 2, were suitable for this requirement.

The piston was used to enforce the sinusoidal input pressure, however, there was the risk of the piston and bubble "decoupling" at high sinusoidal frequencies and acting as a two degree of freedom (DoF) system, where the piston's own natural frequency in the system becomes more dominant. If the piston and bubble interacted as a two DoF system, the amplitude of the bubble's oscillations could not be reliably analyzed. Ideally, we should perform simulations in which the effect of the piston's inertia is negligible.

The ratio of the piston's inertia to the driving pressure was also derived in the supplementary material:

$$\beta = \frac{m_p \pi R_0^3 \Omega_d}{A_p^2 \mu}, \tag{4}$$

where β is our dimensionless piston inertia number. Ideally, $\beta \ll 1$, for forcing frequencies close to the natural frequency $\Omega_d \approx \omega_0$. Eq. (4) was derived for a spherical bubble, but can be approximated for a surface nanobubble by setting $R_0 = R_{eq,0}$ again. Interestingly, this dimensionless number does not depend on pressure amplitude ΔP_∞, but instead depends on the forcing frequency Ω_d, and the viscosity μ. The mass and area of the piston is important with a lighter and larger piston most likely to avoid these adverse effects. While there is an A_p^2 term in the denominator, the piston mass is typically dependent on the plane area, so the number typically scales with $m_p/A_p^2 \propto 1/A_p$ for a fixed piston density. For oscillations near the peak frequency $\Omega_d \approx 70\,\mathrm{rad/ns}$ (see Section III), $\beta \approx 0.056$, which we assume is low enough to neglect the piston's inertia.

III. RESULTS AND DISCUSSIONS

Fourteen MD simulations were run with surface nanobubbles subjected to pressure oscillations of the form $P_\infty(t) = P_{\infty,0} + \Delta P_\infty \sin(\Omega_d t)$, at varying driving frequencies between $\Omega_d = 10\,\mathrm{rad/ns}$ and $\Omega_d = 120\,\mathrm{rad/ns}$, chosen to be of similar order of magnitude to the natural frequency of an equivalent sized spherical nanobubble (see Eq. (9)). The pressure amplitude was kept at $\Delta P_\infty = 5\,\mathrm{MPa}$, which is relatively large to allow measurable changes in the bubble size in the MD simulations, although was found to be small enough to not cause strong non-linear effects in the bubble's response.

For the slowest oscillation case, $\Omega_d = 10\,\mathrm{rad/ns}$, the inertial and viscous forces of the surrounding liquid can be neglected, and the bubble response is expressed solely in terms of the pressure balance across the liquid–gas interface:

$$P_{g,0}\left(\frac{V_0}{V}\right)^k - (P_{\infty,0} + \Delta P_\infty \sin(\Omega_d t) - P_v) - \frac{4\gamma \sin\theta}{L} = 0, \tag{5}$$

for a spherical cap with volume:

$$V = \frac{\pi L^3}{24 \sin^3\theta}(1 - \cos\theta)^2(2 + \cos\theta), \tag{6}$$

and V_0 equal to the initial volume.[33] Eq. (5) is equivalent to the pressure balance (in the square brackets) on the right hand side of Eq. (1), but now is applicable for a surface nanobubble. The Laplace pressure $2\gamma/R$ is given by the final term on the left hand side of Eq. (5), with the radius of curvature of a spherical cap given by:

$$R = \frac{L}{2\sin\theta}. \tag{7}$$

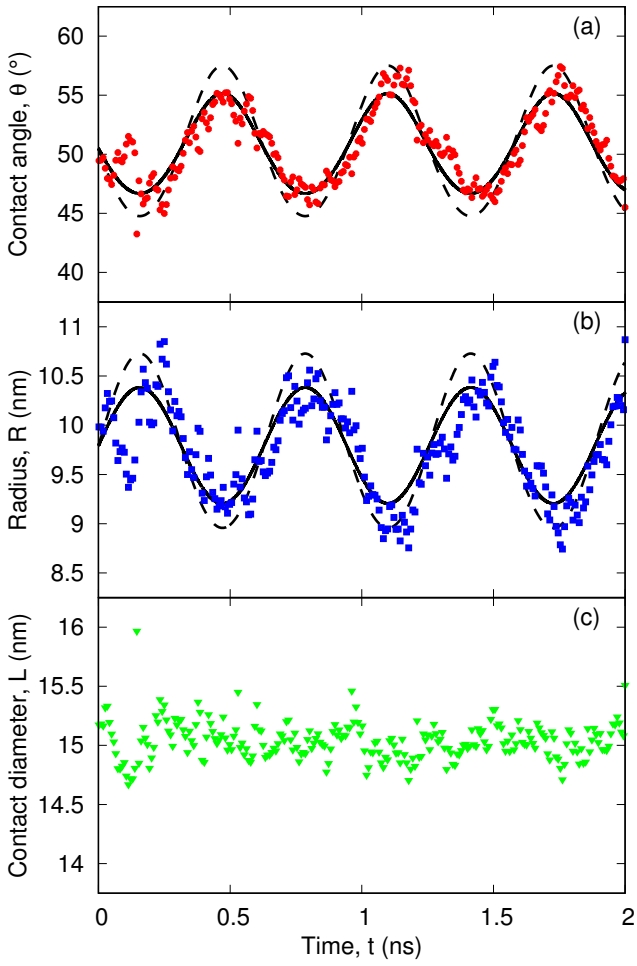

FIG. 3: Variation of the: (a) contact angle θ (red circles), (b) radius of curvature R (blue squares), and (c) lateral contact diameter L (green inverted triangles), from the MD simulations of an oscillating surface nanobubble, with pressure enforced by a sinusoidal input function, $\Delta P_\infty = 5\,\mathrm{MPa}$ and $\Omega_d = 10\,\mathrm{rad/ns}$. Also shown in (a) and (b) is the predicted contact angle and radius of curvature, found using Eqs. (5) and (7), respectively, each with two cases assuming adiabatic ($k = 5/3$, solid black line) and isothermal ($k = 1$, dashed black line) expansion.

The variation in the surface nanobubble's contact angle and radius of curvature with time was solved numerically using Eqs. (5)–(7) and compared to MD results, as shown in Figs. 3(a) and (b), respectively. Also shown is the variation in contact diameter L in Fig. 3(c) to show the surface nanobubble remains pinned; the surface nanobubble is clearly in CCR growth mode.

There is also some high-frequency noise present in the MD simulations as can be seen in Fig. 3, which affects the spherical cap fitting. These are most likely caused by thermal fluctuations, which are more prevalent at the nanoscale;[22,69] we would expect the effects of these fluctuations to be negligible for larger surface nanobubbles.

Both Eqs. (1) and (5) assume that the polytropic relation

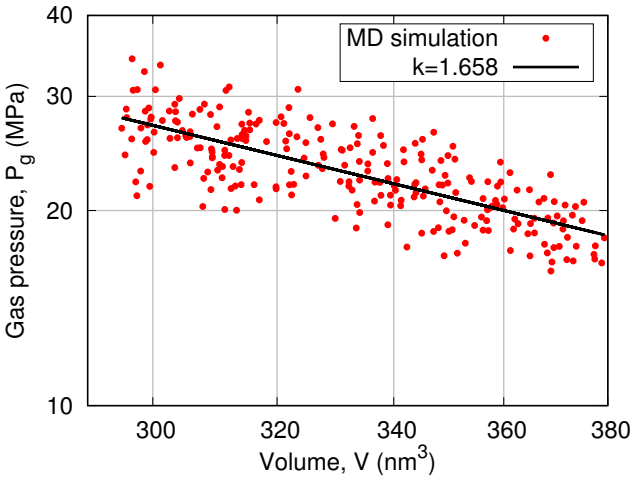

FIG. 4: Variation of gas pressure with bubble volume for a surface nanobubble subjected to an oscillating pressure, with $\Delta P_\infty = 5\,\mathrm{MPa}$ and $\Omega_d = 10\,\mathrm{rad/ns}$, plotted on logarithmic axes. A line is also plotted, corresponding to the fitted polytropic exponent $k = 1.658$.

holds, which implies a fixed mass content of the bubble. This is acceptable for "short" time scales ($\sim 1\,\mathrm{ns}$ for nanobubbles), where growth is driven by the instantaneous difference in gas, liquid and Laplace pressures across the bubble interface.[1] For longer time scales ($\sim 10\,\mu\mathrm{s}$), diffusive dynamics become important, and the surface nanobubble would be expected to gradually grow via the net influx of gas molecules across the liquid–gas interface, driven by the surrounding liquid's supersaturation variation with pressure, i.e. rectified diffusion.[28,59,70,71] For the purposes of this work, we neglect the effects of diffusive growth, due to the short timescales modeled in the MD simulations.

The polytropic exponent k during growth is dependent on both the bubble's current size and growth rate,[35,36] and was found by fitting a line to the variation of gas pressure with bubble volume, as shown in Fig. 4. This polytropic exponent can qualitatively describe the thermodynamic behavior of the gas, with $k = 1$ indicating isothermal expansion, and $k = 5/3 \approx 1.6667$ being adiabatic expansion for a monatomic gas.[72] The fitted value $k = 1.658$ is very close to the adiabatic limit, and so we assume adiabatic expansion in the $\Omega_d = 10\,\mathrm{rad/ns}$ oscillation case. The MD results are in better agreement with the adiabatic prediction in Figs. 3(a) and (b), as expected from the fitted value of k.

Prosperetti [35,36] analyzed the thermal behavior and effective damping of the internal gas phase for spherical bubble oscillations in terms of the Péclet number $Pe = R_0^2\Omega_d/D_g$. The thermal diffusivity of the gas is given by $D_g = K_g/\rho_g C_p$, where K_g is the thermal conductivity, ρ_g is the gas density, and C_p is the specific heat capacity at constant pressure. Prosperetti [35,36] suggested that for $Pe \lesssim 1$, the gas expansion can be considered isothermal, while adiabatic behavior would be expected for Péclet numbers approaching $\sim 10^5$. For the bubble cases run here, with the gas initially at $P_{g,0} = 23.4\,\mathrm{MPa}$,

$Pe \approx 7$ for the slowest oscillation frequency $\Omega_d = 10\,\mathrm{rad/ns}$.[55] For such a small bubble close to the solid it may seem surprising that the observed gas behavior in Fig. 4 is not isothermal, since the Péclet number is not much greater than 1. However, it should be noted that with the current MD simulation setup, the LJ solid atoms of the lower substrate are kept rigid. This effectively creates an insulated boundary, where no heat transfer is possible across the gas–solid interface, and this could artificially lead the gas to more adiabatic behavior. If the substrate was thermostatted like the liquid, it might result in nearer isothermal gas expansion, which could be investigated in future work. Heat transfer between the liquid and gas phases could also have been inhibited by nanoscale interfacial phenomena, such as the Kapitza resistance, not considered in the analyses by Prosperetti [35,36]. The slowest oscillation case exhibited near adiabatic behavior, as shown in Figs. 3 and 4, so for the rest of the oscillating pressure cases it was assumed all the bubbles expanded adiabatically, since Pe continues to increase with increasing Ω_d.[36]

The variation of the pressures acting on the bubble as it oscillated at $\Omega_d = 10\,\mathrm{rad/ns}$ in the MD simulation was also well predicted by the proposed models, as shown in Fig. 5(a). The liquid pressure variation closely matched the sinusoidal input function applied from the piston. The gas and Laplace pressure terms were found to be well predicted by Eq. (5), as shown in Figs. 5(b) and (c), respectively.

For all driving frequency cases, the surface nanobubble oscillated with pinned CCR growth mode; the contact angle variations all exhibited an oscillatory response and a sinusoidal function could be fitted in each case. The contact angle oscillation amplitude was measured, and is shown as a function of driving frequency in Fig. 6. The oscillation amplitude of the surface nanobubble from the MD simulations is maximum around $\Omega_d = 70\,\mathrm{rad/ns}$. By classical harmonic oscillator theory, this peak oscillation frequency must be lower than the system's natural frequency, due to damping which could arise from viscous stresses at the liquid–gas interface, dissipation in the viscous boundary layer across the solid, and acoustic radiation.[35,36,38–40] Various models in literature have been proposed to estimate the natural frequencies for a spherical bubble, CCA surface bubble, and gas entrapped within a cylindrical micropore, as will be discussed below with comparisons to our MD results.[34,37,39]

The simplest estimate for the bubble's natural frequency can be found by linearizing Eq. (1) for small radial perturbations ξ, i.e. $R(t) = R_0 + \xi(t)$, where $\dot{R} = \dot{\xi}$, and $\ddot{R} = \ddot{\xi}$. Ignoring higher orders of ξ, a simplified expression for the spherical bubble's oscillation dynamics can be obtained:

$$\ddot{\xi} + \frac{4\nu}{R_0^2}\dot{\xi} + \frac{1}{\rho R_0^2}\left[3kP_{g,0} - \frac{2\gamma}{R_0}\right]\xi = \frac{\Delta P_\infty}{\rho R_0} f(t), \qquad (8)$$

where $f(t)$ is some time dependent function, e.g. a sinusoidal function, as used in these simulations. Eq. (8) resembles the classical equation for a damped oscillator $\ddot{x} + \alpha\dot{x} + \omega_0^2 x = F(t)$, where x is a generic coordinate frame, ω_0 is the system natural frequency, α is the damping coefficient, and $F(t)$ is the forcing function.

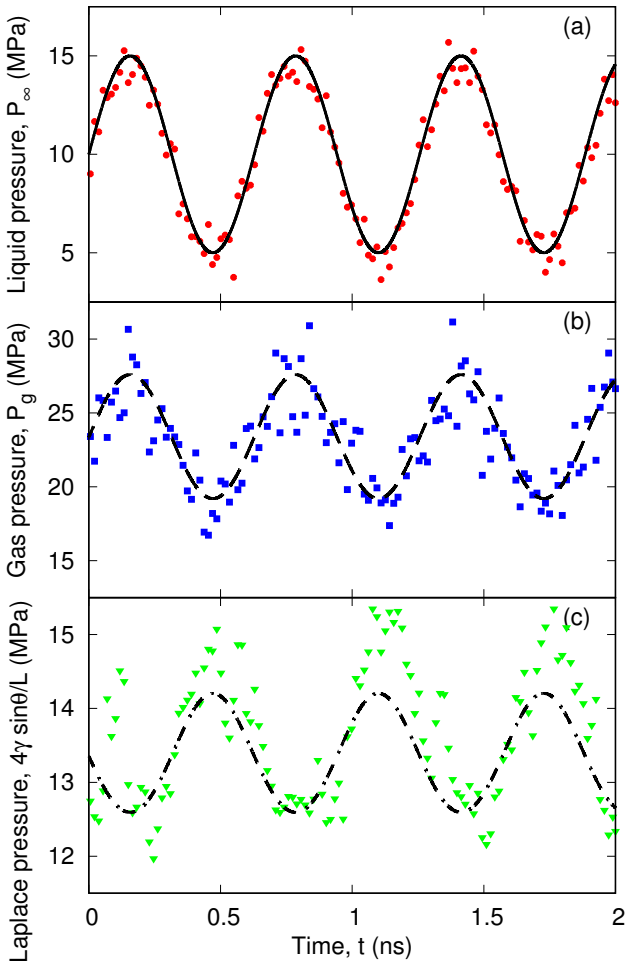

FIG. 5: Time variation of: (a) liquid pressure (red circles, solid line), (b) surface nanobubble gas pressure (blue squares, dashed line), and (c) Laplace pressure (green inverted triangles, dot-dashed line), for an oscillating pressure MD simulation, with $\Delta P_\infty = 5\,\mathrm{MPa}$ and $\Omega_d = 10\,\mathrm{rad/ns}$. The different pressure contribution terms from Eq. (5) are shown as lines, assuming adiabatic expansion $k = 5/3$, and MD simulation results are represented as symbols.

The natural frequency of a spherical bubble can be found from Eq. (8):

$$\omega_{0,M} = \left[\frac{3kP_{g,0} - 2\gamma/R_0}{\rho R_0^2}\right]^{\frac{1}{2}}, \qquad (9)$$

where $P_{g,0} = P_{\infty,0} - P_v + 2\gamma/R_0$. Minnaert [34] first derived the natural frequency of a spherical bubble, without surface tension effects, which can be obtained from Eq. (9) by setting $\gamma = 0$. Due to its similar form, Eq. (9) is also referred to as the Minnaert frequency, although modified to account for the effects of surface tension. Eq. (9) predicts the natural frequency of the spherical nanobubble to be $\omega_{0,M} = 32.8\,\mathrm{rad/ns}$, using the surface nanobubble's radius of curvature from Eq. (7) and assuming adiabatic expansion as discussed earlier. Fig. 6 clearly shows peak oscillations for the surface nanobubbles

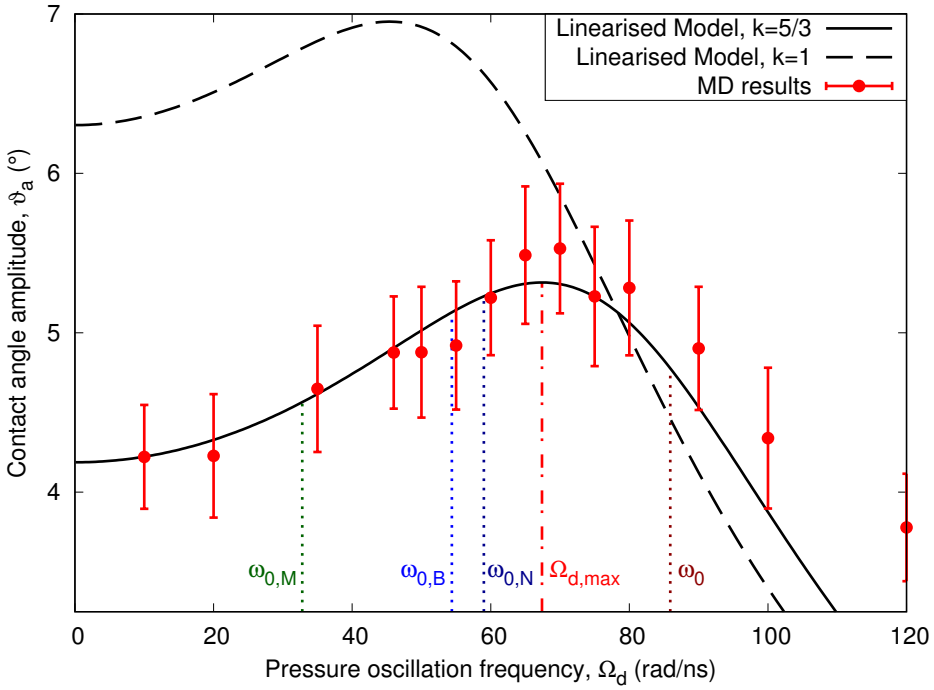

FIG. 6: Variation in the surface nanobubble contact angle amplitude, with pressure oscillation frequency Ω_d. The MD simulations are compared with the oscillation amplitude of the linearized model in Eq. (14) for various values of k, assuming adiabatic ($k = 5/3$) and isothermal ($k = 1$) expansion. The natural frequency ω_0 and oscillation frequency for maximum amplitude $\Omega_{d,max}$ are shown, predicted from Eqs. (15) and (16), respectively. Also labelled are the Minnaert frequency $\omega_{0,M}$, Blue frequency $\omega_{0,B}$ (both modified to account for surface tension), and Miller–Nyborg frequency $\omega_{0,N}$, from Eqs. (9), (10) and (11), respectively.[34,37,39] The full MD results, with comparisons to Eq. (12), for each of the oscillation pressure cases can be found in the supplementary material.

in our MD simulations at frequencies approximately double this Minnaert frequency, so we conclude that the Minnaert frequency is not suitable for predicting the surface nanobubble's natural frequency.

The natural frequency of a surface bubble expanding with CCA growth mode was derived by Blue[37]:

$$\omega_{0,B} = \left[\frac{3kP_{g,0} - 2\gamma/R_0}{\rho R_0^2 (1-\cos\theta_0)}\right]^{\frac{1}{2}}. \tag{10}$$

Eq. (10) has been modified from Ref. 37 to include the effects of surface tension again, and the $(1-\cos\theta_0)$ term in the denominator accounts for the bubble's spherical cap shape. Eq. (10) predicts the natural frequency of the surface nanobubble to be $\omega_{0,B} = 54.4\,\mathrm{rad/ns}$, which is larger than the Minnaert frequency but still less than the peak observed in the MD results as shown in Fig. 6. Similar to spherical bubble growth, models based on CCA growth for spherical capped bubbles assume that the radius of curvature increases with bubble size, and so does not properly account for the Laplace pressure variation of the pinned surface nanobubble during oscillations.

Previous investigations into pinned nano and microbubble resonance has so far been dominated by gas trapped in micropores.[39,40,68] Most of these analyses differ from this work in that they generally assume a flat liquid–gas interface at equilibrium and that during oscillation the interface profile is parabolic, rather than maintaining a spherical cap profile. The most commonly used micropore model is by Miller and Nyborg[39]:

$$\omega_{0,N} = \left[\frac{480\pi\gamma h + 15\pi k P_{\infty,0} L^2}{16\rho L^3 h}\right]^{\frac{1}{2}}, \tag{11}$$

where h is the depth of the cylindrical pore, with diameter L. For our application, we define the micropore depth with equivalent volume to the surface nanobubble, i.e. $h = 4V_0/\pi L^2$. Since it is assumed a flat interface at equilibrium, the initial gas pressure would be expected to be equal to the external liquid pressure, hence the $P_{\infty,0}$ term in Eq. (11). Surface nanobubble pressures typically exceed the external liquid pressure by up to $\sim 1\,\mathrm{MPa}$.[9,25,33,73] Eq. (11) predicts $\omega_{0,N} = 59.0\,\mathrm{rad/ns}$, which is higher than the previous Minnaert frequency and Blue frequency models, but still lower than the peak from the MD simulations, as shown in Fig. 6.

Eqs. (9)–(11) all contain a pressure and surface tension term in the numerator, which roughly corresponds to the "stiffness" of the bubble. The gas stiffness follows from the polytropic law, which requires the initial bubble pressure and volume to be properly evaluated. The surface tension term derives from the Laplace pressure during oscillation, and we need to cap-

ture this specific variation during pinned CCR growth.[33] None of these equations captures all three of these properties, which is why they fail to provide a suitable estimate for the surface nanobubble natural frequency, which must exceed the peak frequency value observed in Fig. 6.

Instead, we have derived a simple model for the damped CCR oscillations of the surface nanobubbles in the supplementary material:

$$\ddot{\vartheta} + \frac{4\nu}{R_{eq,0}^2}\dot{\vartheta} + \frac{1}{\rho R_{eq,0}^2}\left[3kP_{g,0} + \frac{4\gamma\sin\theta_0}{L}\cos\theta_0\,(2+\cos\theta_0)\right]\vartheta = \Delta P_\infty \frac{(2+\cos\theta_0)\sin\theta_0}{\rho R_{eq,0}^2} f(t), \quad (12)$$

where $\theta(t) = \theta_0 + \vartheta(t)$ and equivalent radius for a spherical cap is $R_{eq,0} = (3V_0/4\pi)^{1/3}$, or:

$$R_{eq,0} = \frac{L}{2\sin\theta_0}\left[\frac{1}{4}(1-\cos\theta_0)^2(2+\cos\theta_0)\right]^{\frac{1}{3}}. \quad (13)$$

Eq. (12) is adapted from Leighton's "volume-frame" Rayleigh–Plesset equation,[74] modified for a CCR oscillating spherical cap bubble, with the pressure balance of the form in Eq. (5). As such, we accurately capture the appropriate bubble volume, pressure and Laplace pressure effects on the stiffness as discussed above, although the inertial and viscous contributions are only approximated. Numerical simulations, for example with potential flow or Stokes flow, could be performed for the complete description of the surrounding liquid flow around these constrained bubbles.[38,40] We ignore any of the inertial or viscous effects of the gas phase, as these are dominated by the surrounding liquid phase.[1] We note that the $4\nu\dot{\vartheta}/R_{eq,0}^2$ damping term in Eq. (12) only captures equivalent viscous stresses at the liquid–gas interface, as is the case in Eq. (1), and does not capture dissipation from the boundary layer across the solid, nor acoustic radiation.[38–40] We estimate the ratio of viscous damping at the liquid–gas interface to the dissipation in the boundary layer across the solid approximately equal to $\sqrt{2048\nu/L^2\Omega_d} \approx 17.8$,[39] when $\Omega_d \approx 10\,\mathrm{rad/ns}$, and so we do not consider these additional dissipation effects significant in our case.

For oscillations driven by a sinusoidal pressure field, i.e. $f(t) = \sin(\Omega_d t)$, the amplitude of the bubble oscillations is:

$$\vartheta_a = \frac{p_a}{\sqrt{\left(\Omega_d^2 - \omega_0^2\right)^2 + \alpha^2\Omega_d^2}}, \quad (14)$$

where $p_a = \Delta P_\infty(2+\cos\theta_0)\sin\theta_0/\rho R_{eq,0}^2$ and $\alpha = 4\nu/R_{eq,0}^2$ from Eq. (12), and with natural frequency:

$$\omega_0 = \left[\frac{3kP_{g,0} + (4\gamma\sin\theta_0/L)\cos\theta_0\,(2+\cos\theta_0)}{\rho R_{eq,0}^2}\right]^{\frac{1}{2}}, \quad (15)$$

and a maximum amplitude at frequency:

$$\Omega_{d,max} = \sqrt{\omega_0^2 - \frac{\alpha^2}{2}}. \quad (16)$$

Eq. (15) has a similar form to Eqs. (9)–(11). There is a $3kP_{g,0}$ term that contributes to the system stiffness, however, the surface tension contributions now differ. In Eq. (15) the Laplace pressure term has a different sign to that in Eqs. (9) and (10), which is a result of the pinned contact line and CCR growth mode. This change in sign means an increase in the natural frequency of the surface nanobubble, while the $R_{eq,0}$ term in the denominator accounts for the spherical cap shape. Our proposed natural frequency model is compared with the models of Minnaert, Blue, and Miller and Nyborg in Table III, with summaries of their underlying assumptions.

Eqs. (15) and (16) predict the natural and peak oscillation frequencies to be $\omega_0 = 85.9\,\mathrm{rad/ns}$ and $\Omega_{d,max} = 67.4\,\mathrm{rad/ns}$, respectively, assuming adiabatic expansion, as shown in Fig. 6. This is close to the MD simulations which show the expected peak oscillation frequency to be in between $\Omega_d = 65\,\mathrm{rad/ns}$ and $\Omega_d = 70\,\mathrm{rad/ns}$.

Eq. (14) predicts the amplitude–frequency variation, and is in reasonably good agreement with the MD simulations for low frequencies. The agreement with the MD results breaks down above the predicted natural frequency, due to the inertial contributions becoming more dominant, as well as possible higher oscillation modes; further numerical modeling would be required to accurately resolve these dynamics. This increasing discrepancy could also be due to the dimensionless number β, as discussed in Section II, increasing with frequency; for $\Omega_d = 120\,\mathrm{rad/ns}$, we have $\beta \approx 0.1$, and so the piston inertia might be influencing the surface nanobubble's oscillation dynamics.

Also shown in Fig. 6 is the predicted response for isothermal expansion $k = 1$, which shows the peak oscillation frequency would decrease, although with an increased oscillation amplitude at lower frequencies. The distribution of the MD results is in better agreement assuming adiabatic expansion, as opposed to isothermal expansion. This also follows from the earlier discussions, where the slowest oscillation case exhibited near adiabatic expansion.

The criterion $\omega_0^2 - \alpha^2/2 > 0$ is required for an "underdamped" bubble from Eq. (16), such that $\Omega_{d,max} > 0$ and not complex, which is clearly shown in Fig. 6. The peak oscillation frequency is a result of the surface nanobubble's high internal gas pressure that counteracts the strong effects of viscosity at the nanoscale.[20–22] The underdamped case can also be obtained for spherical nanobubbles in more realistic fluid conditions, e.g. $P_{\infty,0} = 0.1\,\mathrm{MPa}$, $\gamma = 71.69\,\mathrm{mJ/m^2}$, $\mu = 8.53\times10^{-4}\,\mathrm{Pa\,s}$[55] and $R_0 = 20\,\mathrm{nm}$, where $\alpha = 4\nu/R_0^2$ from Eq. (8), and natural frequency from Eq. (9) are used in Eq. (16) instead. The natural frequency and peak amplitude frequency would now be $\omega_{0,M} = 8.5\,\mathrm{rad/ns}$ and $\Omega_{d,max} = 6.0\,\mathrm{rad/ns}$, respectively, for the spherical nanobubble, and so the peak frequency observed in Fig. (6) is not a particularly anomalous result.

We assumed for our proposed natural frequency model in Eq. (15) that the bubble retains a spherical cap shape during its pinned oscillation mode. The Weber number can assess the relative effects of the inertial forces against the surface tension, $We = \rho R_0^3\omega_0^2/\gamma$; Prosperetti[38] used the square root of this Weber number to non-dimensionalise the frequency of

TABLE III: Comparisons of the Minnaert, Blue, and Miller–Nyborg natural frequency models, with our own model proposed in this paper. The Minnaert and Blue frequency models are both modified from their original reference to account for the effects of surface tension.

Model	Natural frequency	Eq. number	Assumptions	Ref.
Minnaert	$\omega_{0,M} = \left[\frac{3kP_{g,0} - 2\gamma/R_0}{\rho R_0^2}\right]^{\frac{1}{2}}$	(9)	Spherical bulk bubble; radial expansion.	34
Blue	$\omega_{0,B} = \left[\frac{3kP_{g,0} - 2\gamma/R_0}{\rho R_0^2 (1-\cos\theta_0)}\right]^{\frac{1}{2}}$	(10)	Spherical cap surface bubble; unpinned CCA expansion.	37
Miller–Nyborg	$\omega_{0,N} = \left[\frac{480\pi\gamma h + 15\pi k P_{\infty,0} L^2}{16\rho L^3 h}\right]^{\frac{1}{2}}$	(11)	Pinned micro-pore bubble; parabolic oscillation profile about mean flat interface position.	39
Proposed here	$\omega_0 = \left[\frac{3kP_{g,0} + (4\gamma\sin\theta_0/L)\cos\theta_0\,(2+\cos\theta_0)}{\rho R_{eq,0}^2}\right]^{\frac{1}{2}}$	(15)[a]	Spherical cap surface bubble; pinned CCR expansion.	–

[a] Additionally, from Eq. (13), $R_{eq,0} = \frac{L}{2\sin\theta_0}\left[\frac{1}{4}(1-\cos\theta_0)^2(2+\cos\theta_0)\right]^{\frac{1}{3}}$

constrained spherical droplets and bubbles. For our MD simulation case, setting $R_{eq,0} = R_0$, we obtain $We \approx 10$. For larger bubbles the relative effects of the surface tension would be reduced, although this spherical cap assumption is also essential for the natural frequency of a surface bubble undergoing CCA growth mode, as in Eq. (10). This mode was observed by Blue[37], who performed experiments of $R_0 \approx 70\,\mu$m CCA surface bubbles oscillating at frequencies ≈ 35 kHz, equivalent to $We \approx 230$. We suggest our proposed natural frequency model is also suitable at comparable Weber numbers, due to the similar assumptions taken in Ref. 37, and provided that the contact line remains pinned. Eq. (12) may also need to be modified to account for additional viscous dissipation across the solid for oscillations of larger surface nanobubbles as discussed earlier,[39] as well as possible diffusive growth effects for long-term pressure oscillations.[71]

IV. CONCLUSIONS

We performed Molecular Dynamics (MD) simulations of surface nanobubbles subjected to pressures oscillating in the range of 10 to 120 rad/ns. The surface nanobubbles were confirmed to oscillate with a constant contact radius (CCR) mode of growth, due to their pinned contact line.

Despite strong viscous effects at the nanoscale, we could identify a peak oscillation amplitude in the frequency response, characteristic of an "underdamped" system, which was driven by the surface nanobubble's high internal gas pressure. We assumed this peak frequency to be at least lower than the system's natural frequency, due to damping from viscous stresses at the bubble surface, as assumed in the Rayleigh–Plesset equation, as well as viscous boundary layer dissipation across the solid substrate and acoustic dissipation from the oscillating interface.[35,36,38–40]

We estimated different natural frequencies based on the assumptions of: a free spherical bubble, a constant contact angle (CCA) surface bubble, and a bubble entrapped in a cylindrical micropore, adapted from Ref. 34, 37 and 39, respectively. We determined that the natural frequency model had to account for the surface nanobubble's spherical cap volume, high internal pressure, and pinned growth mode. We modified the volume-frame Rayleigh–Plesset model from Ref. 74 to approximate the inertial and viscous contributions for CCR oscillation dynamics, which was used to predict the natural frequency and amplitude–frequency response of our surface nanobubble.

It was found that the bubbles expanded with near adiabatic behavior in the MD simulations, despite their small size and close proximity to the liquid and solid surfaces, which would suggest more isothermal conditions.[35,36] We note that the effect of the rigid solid atoms in our MD simulations could have provided an insulating effect on the internal gas phase, which would have led to zero heat transfer across the gas–solid interface. Future work could investigate how the solid temperature influences the surface nanobubble's thermal expansion behavior, as well as the possible thermal (Kapitza) resistance across the liquid–gas interface.

Further simulations could be run with a pinned contact line, although with larger fluid domains to more accurately capture the fluid dynamics of the surrounding liquid, and verify the proposed oscillation models at different scales. Future work could also investigate the long-term oscillations of these surface nanobubbles, approaching diffusive time scales where the bubbles could gain mass via rectified diffusion.[71]

We encourage more experimental investigations of surface nanobubble oscillation dynamics, to compare to our proposed models. Surface nanobubbles could be stimulated with ultrasound transducers, similar to the application in ultrasound agents, however, the required GHz frequencies may be higher than the realistic range of current equipment.[11] Alternatively, the substrate could be driven to these frequencies with laser pulses,[75] although we understand again that the measurement apparatus would need to be highly sensitive to capture such nanoscale signals.

SUPPLEMENTARY MATERIAL

See the supplementary material for a PDF containing the derivation of our proposed model in Eq. (12), the derivations of inertial length scales and dimensionless numbers for the suitability of our MD domains, and MD simulation results at all oscillation frequencies, with fitted sine wave profile and results from our proposed model.

ACKNOWLEDGMENTS

This work is supported in the UK by the Engineering and Physical Sciences Research Council (EPSRC) under grants EP/N016602/1 and EP/R007438/1. All MD simulations were run on ARCHER, the UK's national supercomputing service. Declaration of Interests. The authors report no conflict of interest. We thank the reviewers of this paper for their helpful comments. The authors would like to dedicate this paper to Prof Jason Reese, our colleague, mentor and friend, who passed away in March 2019.

DATA AVAILABILITY

The data that support the findings of this study are openly available from [*doi to be confirmed upon acceptance of manuscript*].

REFERENCES

[1]C. E. Brennen, *Cavitation and Bubble Dynamics* (Cambridge University Press, 2013).
[2]E. Y. Lukianova-Hleb, X. Ren, R. R. Sawant, X. Wu, V. P. Torchilin, and D. O. Lapotko, "On-Demand Intracellular Amplification of Chemoradiation with Cancer-Specific Plasmonic nanobubbles," Nat. Med. **20**, 778–784 (2014).
[3]E. Y. Lukianova-Hleb, Y.-S. Kim, I. Belatsarkouski, A. M. Gillenwater, B. E. O'Neill, and D. O. Lapotko, "Intraoperative diagnostics and elimination of residual microtumours with plasmonic nanobubbles," Nat. Nanotechnol. **11**, 525–532 (2016).
[4]A. Delalande, S. Kotopoulis, M. Postema, P. Midoux, and C. Pichon, "Sonoporation: Mechanistic insights and ongoing challenges for gene transfer," Gene **525**, 191–199 (2013).
[5]A. Agarwal, W. J. Ng, and Y. Liu, "Principle and Applications of Microbubble and Nanobubble Technology for Water Treatment," Chemosphere **84**, 1175–1180 (2011).
[6]M. Dular, T. Griessler-Bulc, I. Gutierrez-Aguirre, E. Heath, T. Kosjek, A. Krivograd Klemenčič, M. Oder, M. Petkovšek, N. Rački, M. Ravnikar, A. Šarc, B. Širok, M. Zupanc, M. Žitnik, and B. Kompare, "Use of hydrodynamic cavitation in (waste)water treatment," Ultrason. Sonochem. **29**, 577–588 (2016).
[7]F. Hui, B. Li, P. He, J. Hu, and Y. Fang, "Electrochemical fabrication of nanoporous polypyrrole film on HOPG using nanobubbles as templates," Electrochem. Commun. **11**, 639–642 (2009).
[8]C. Huang, J. Jiang, M. Lu, L. Sun, E. I. Meletis, and Y. Hao, "Capturing Electrochemically Evolved Nanobubbles by Electroless Deposition. A Facile Route to the Synthesis of Hollow Nanoparticles," Nano Lett. **9**, 4297–4301 (2009).
[9]D. Lohse and X. Zhang, "Surface Nanobubbles and Nanodroplets," Rev. Mod. Phys. **87**, 981–1035 (2015).
[10]S. Brems, M. Hauptmann, E. Camerotto, A. Pacco, T.-G. Kim, X. Xu, K. Wostyn, P. Mertens, and S. De Gendt, "Nanoparticle Removal with Megasonics: A Review," ECS J. Solid State Sci. Technol. **3**, N3010–N3015 (2014).
[11]E. Stride and N. Saffari, "Microbubble ultrasound contrast agents: A review," Proc. Inst. Mech. Eng., Part H **217**, 429–447 (2003).
[12]S. Martynov, E. Kostson, N. Saffari, and E. Stride, "Forced vibrations of a bubble in a liquid-filled elastic vessel," J. Acoust. Soc. Am. **130**, 2700–2708 (2011).
[13]M. S. Plesset, "The dynamics of cavitation bubbles," J. Appl. Mech. **16**, 277–282 (1949).
[14]T. B. Benjamin and A. T. Ellis, "The Collapse of Cavitation Bubbles and the Pressures thereby Produced against Solid Boundaries," Philos. Trans. R. Soc., A **260**, 221–240 (1966).
[15]S. Zhang and J. H. Duncan, "On the nonspherical collapse and rebound of a cavitation bubble," Phys. Fluids **6**, 2352–2362 (1994).
[16]P. Koukouvinis, M. Gavaises, O. Supponen, and M. Farhat, "Numerical simulation of a collapsing bubble subject to gravity," Phys. Fluids **28**, 032110 (2016).
[17]O. Supponen, D. Obreschkow, M. Tinguely, P. Kobel, N. Dorsaz, and M. Farhat, "Scaling laws for jets of single cavitation bubbles," J. Fluid Mech. **802**, 263–293 (2016).
[18]J. Lombard, T. Biben, and S. Merabia, "Kinetics of Nanobubble Generation Around Overheated Nanoparticles," Phys. Rev. Lett. **112**, 105701 (2014).
[19]K. Manmi and Q. Wang, "Acoustic microbubble dynamics with viscous effects," Ultrason. Sonochem. **36**, 427–436 (2017).
[20]J. Dzubiella, "Interface dynamics of microscopic cavities in water," J. Chem. Phys. **126**, 194504 (2007).
[21]R. Hołyst, M. Litniewski, and P. Garstecki, "Large-scale molecular dynamics verification of the Rayleigh-Plesset approximation for collapse of nanobubbles," Phys. Rev. E **82**, 066309 (2010).
[22]G. Menzl, M. A. Gonzalez, P. Geiger, F. Caupin, J. L. F. Abascal, C. Valeriani, and C. Dellago, "Molecular Mechanism for Cavitation in Water Under Tension," Proc. Natl. Acad. Sci. U. S. A. **113**, 13582–13587 (2016).
[23]V. H. Man, M. S. Li, P. Derreumaux, and P. H. Nguyen, "Rayleigh-Plesset equation of the bubble stable cavitation in water: A nonequilibrium all-atom molecular dynamics simulation study," J. Chem. Phys. **148**, 094505 (2018).
[24]N. Ishida, T. Inoue, M. Miyahara, and K. Higashitani, "Nano Bubbles on a Hydrophobic Surface in Water Observed by Tapping-Mode Atomic Force Microscopy," Langmuir **16**, 6377–6380 (2000).
[25]X. H. Zhang, A. Quinn, and W. A. Ducker, "Nanobubbles at the Interface between Water and a Hydrophobic Solid," Langmuir **24**, 4756–4764 (2008).
[26]Y. Liu and X. Zhang, "Nanobubble stability induced by contact line pinning," J. Chem. Phys. **138**, 014706 (2013).
[27]H. An, G. Liu, R. Atkin, and V. S. J. Craig, "Surface Nanobubbles in Nonaqueous Media: Looking for Nanobubbles in DMSO, Formamide, Propylene Carbonate, Ethylammonium Nitrate, and Propylammonium Nitrate," ACS Nano **9**, 7596–7607 (2015).
[28]D. Lohse and X. Zhang, "Pinning and gas oversaturation imply stable single surface nanobubbles," Phys. Rev. E **91**, 031003 (2015).
[29]P. Attard, "Pinning Down the Reasons for the Size, Shape, and Stability of Nanobubbles," Langmuir **32**, 11138–11146 (2016).
[30]A. Azevedo, R. Etchepare, S. Calgaroto, and J. Rubio, "Aqueous dispersions of nanobubbles: Generation, properties and features," Miner. Eng. **94**, 29–37 (2016).
[31]P. E. Theodorakis and Z. Che, "Surface nanobubbles: Theory, simulation, and experiment. A review," Adv. Colloid Interface Sci. **272**, 101995 (2019).
[32]B. M. Borkent, S. M. Dammer, H. Schönherr, G. J. Vancso, and D. Lohse, "Superstability of Surface Nanobubbles," Phys. Rev. Lett. **98**, 204502 (2007).
[33]D. Dockar, M. K. Borg, and J. M. Reese, "Mechanical Stability of Surface Nanobubbles," Langmuir **35**, 9325–9333 (2019).
[34]M. Minnaert, "XVI. On musical air-bubbles and the sounds of running water," London, Edinburgh Dublin Philos. Mag. J. Sci. **16**, 235–248 (1933).
[35]A. Prosperetti, "Thermal effects and damping mechanisms in the forced radial oscillations of gas bubbles in liquids," J. Acoust. Soc. Am. **61**, 17–27 (1977).
[36]A. Prosperetti, "The thermal behaviour of oscillating gas bubbles," J. Fluid Mech. **222**, 587–616 (1991).

[37] J. E. Blue, "Resonance of a Bubble on an Infinite Rigid Boundary," J. Acoust. Soc. Am. **41**, 369–372 (1967).
[38] A. Prosperetti, "Linear oscillations of constrained drops, bubbles, and plane liquid surfaces," Phys. Fluids **24**, 032109 (2012).
[39] D. L. Miller and W. L. Nyborg, "Theoretical investigation of the response of gas-filled micropores and cavitation nuclei to ultrasound," J. Acoust. Soc. Am. **73**, 1537–1544 (1983).
[40] H. Gelderblom, A. G. Zijlstra, L. van Wijngaarden, and A. Prosperetti, "Oscillations of a gas pocket on a liquid-covered solid surface," Phys. Fluids **24**, 122101 (2012).
[41] J. H. Weijs, J. H. Snoeijer, and D. Lohse, "Formation of Surface Nanobubbles and the Universality of Their Contact Angles: A Molecular Dynamics Approach," Phys. Rev. Lett. **108**, 104501 (2012).
[42] S. Maheshwari, M. van der Hoef, X. Zhang, and D. Lohse, "Stability of Surface Nanobubbles: A Molecular Dynamics Study," Langmuir **32**, 11116–11122 (2016).
[43] S. Maheshwari, M. van der Hoef, J. Rodríguez Rodríguez, and D. Lohse, "Leakiness of Pinned Neighboring Surface Nanobubbles Induced by Strong Gas-Surface Interaction," ACS Nano **12**, 2603–2609 (2018).
[44] Z. Che and P. E. Theodorakis, "Formation, dissolution and properties of surface nanobubbles," J. Colloid Interface Sci. **487**, 123–129 (2017).
[45] X. Zhu, R. Verzicco, X. Zhang, and D. Lohse, "Diffusive interaction of multiple surface nanobubbles: shrinkage, growth, and coarsening," Soft Matter **14**, 2006–2014 (2018).
[46] S. Plimpton, "Fast Parallel Algorithms for Short-Range Molecular Dynamics," J. Comput. Phys. **117**, 1–19 (1995).
[47] S.-T. Lou, Z.-Q. Ouyang, Y. Zhang, X.-J. Li, J. Hu, M.-Q. Li, and F.-J. Yang, "Nanobubbles on Solid Surface Imaged by Atomic Force Microscopy," J. Vac. Sci. Technol., B: Microelectron. Nanometer Struct.–Process., Meas., Phenom. **18**, 2573–2575 (2000).
[48] J. W. G. Tyrrell and P. Attard, "Images of Nanobubbles on Hydrophobic Surfaces and Their Interactions," Phys. Rev. Lett. **87**, 176104 (2001).
[49] While the concentric ring patterning would allow "stick-jump" motion of the contact line, as in our previous work, for these simulations, where the surface nanobubble was to remain on the same pinning site, this patterning was not essential and the same could be achieved by a single patch of hydrophobic (S_o) atoms.
[50] A. Stukowski, "Visualization and Analysis of Atomistic Simulation Data with OVITO–the Open Visualization Tool," Modell. Simul. Mater. Sci. Eng. **18**, 015012 (2010).
[51] V. Molinero and E. B. Moore, "Water Modeled As an Intermediate Element between Carbon and Silicon," J. Phys. Chem. B **113**, 4008–4016 (2009).
[52] B. Coasne, A. Galarneau, F. Di Renzo, and R. J. M. Pellenq, "Molecular Simulation of Nitrogen Adsorption in Nanoporous Silica," Langmuir **26**, 10872–10881 (2010).
[53] R. Sander, *NIST Chemistry WebBook, NIST Standard Reference Database Number 69, Eds. P.J. Linstrom and W.G. Mallard* (National Institute of Standards and Technology, Gaithersburg, 20899, 2017) Chap. Henry's Law Constants.
[54] J. L. F. Abascal and C. Vega, "A General Purpose Model for the Condensed Phases of Water: TIP4P/2005," J. Chem. Phys. **123**, 234505 (2005).
[55] E. W. Lemmon, M. O. McLinden, and D. G. Friend, *NIST Chemistry WebBook, NIST Standard Reference Database Number 69, Eds. P.J. Linstrom and W.G. Mallard* (National Institute of Standards and Technology, Gaithersburg, 20899, 2017) Chap. Thermophysical properties of fluid systems.
[56] F. H. Stillinger and T. A. Weber, "Computer simulation of local order in condensed phases of silicon," Phys. Rev. B **31**, 5262–5271 (1985).
[57] While it is well known that water and nitrogen are polyatomic molecules, the terms "atoms" and "molecules" will be used interchangeably throughout to denote any single-particle body in the MD simulations.
[58] L. Martínez, R. Andrade, E. G. Birgin, and J. M. Martínez, "PACKMOL: A Package for Building Initial Configurations for Molecular Dynamics Simulations," J. Comput. Chem. **30**, 2157–2164 (2009).
[59] C. U. Chan, M. Arora, and C.-D. Ohl, "Coalescence, Growth, and Stability of Surface-Attached Nanobubbles," Langmuir **31**, 7041–7046 (2015).
[60] S. Nosé, "A unified formulation of the constant temperature molecular dynamics methods," J. Chem. Phys. **81**, 511–519 (1984).
[61] W. G. Hoover, "Canonical dynamics: Equilibrium phase-space distributions," Phys. Rev. A **31**, 1695–1697 (1985).
[62] Contact angle is conventionally measured from the liquid side, however, for ease of analysis of the spherical cap shape, the contact angle will refer to the gas side for the remainder of this work.
[63] J. H. Irving and J. G. Kirkwood, "The Statistical Mechanical Theory of Transport Processes. IV. The Equations of Hydrodynamics," J. Chem. Phys. **18**, 817–829 (1950).
[64] B. Shi, S. Sinha, and V. K. Dhir, "Molecular dynamics simulation of the density and surface tension of water by particle-particle particle-mesh method," J. Chem. Phys. **124**, 204715 (2006).
[65] M. S. Green, "Markoff Random Processes and the Statistical Mechanics of Time-Dependent Phenomena. II. Irreversible Processes in Fluids," J. Chem. Phys. **22**, 398–413 (1954).
[66] R. Kubo, "Statistical-Mechanical Theory of Irreversible Processes. I. General Theory and Simple Applications to Magnetic and Conduction Problems," J. Phys. Soc. Jpn. **12**, 570–586 (1957).
[67] E. M. Kirova and G. E. Norman, "Viscosity calculations at molecular dynamics simulations," J. Phys.: Conf. Ser. **653**, 012106 (2015).
[68] R. Bolaños-Jiménez, M. Rossi, D. Fernandez Rivas, C. J. Kähler, and A. Marin, "Streaming flow by oscillating bubbles: quantitative diagnostics via particle tracking velocimetry," J. Fluid Mech. **820**, 529–548 (2017).
[69] S. Perumanath, M. K. Borg, M. V. Chubynsky, J. E. Sprittles, and J. M. Reese, "Droplet Coalescence is Initiated by Thermal Motion," Phys. Rev. Lett. **122**, 104501 (2019).
[70] P. S. Epstein and M. S. Plesset, "On the Stability of Gas Bubbles in Liquid-Gas Solutions," J. Chem. Phys. **18**, 1505–1509 (1950).
[71] A. Brotchie and X. H. Zhang, "Response of interfacial nanobubbles to ultrasound irradiation," Soft Matter **7**, 265–269 (2011).
[72] In reality, nitrogen gas is diatomic, however, the single-site nitrogen (N_2) model used in these simulations is monatomic.
[73] T.-W. Huang, S.-Y. Liu, Y.-J. Chuang, H.-Y. Hsieh, C.-Y. Tsai, W.-J. Wu, C.-T. Tsai, U. Mirsaidov, P. Matsudaira, C.-S. Chang, F.-G. Tseng, and F.-R. Chen, "Dynamics of hydrogen nanobubbles in KLH protein solution studied with in situ wet-TEM," Soft Matter **9**, 8856–8861 (2013).
[74] T. G. Leighton, "The Rayleigh–Plesset equation in terms of volume with explicit shear losses," Ultrasonics **48**, 85–90 (2008).
[75] O. Matsuda and O. B. Wright, "Generation and Observation of GHz–THz Acoustic Waves in Thin Films and Microstructures Using Optical Methods," in *Frontiers in Optical Methods*, Vol. 180, edited by K. Shudo, I. Katayama, and S. Ohno (Springer, Berlin, Heidelberg, 2014) pp. 129–151.